FIV2024
IGUAÇU FALLS, BRAZIL
2-5 JULY 2024

FIV2024: FSI² & FIV + N
10th International Symposium on Fluid-Structure Interactions,
Flow-Sound Interactions, Flow-Induced Vibration & Noise

FIV2024-0069
SENSITIVITY ANALYSIS OF A MATHEMATICAL REDUCED-ORDER MODEL FOR VORTEX-INDUCED MOTIONS OF MULTI-COLUMN FLOATING OFFSHORE WIND TURBINES

Éverton L. de Oliveira[1]
Celso P. Pesce[1]
[1]Laboratório de Mecânica Offshore (LMO), Department of Naval Architecture and Ocean Engineering, Escola Politécnica, University of São Paulo, Av. Prof. Lúcio Martins Rodrigues, Butantã, São Paulo – SP, 05508-020, Brazil
ev_lins@usp.br; ceppesce@usp.br

Giovanni A. Amaral[1,2]
[2]Technomar Engineering, Av. Pedroso de Morais, 631, São Paulo – SP, 05419-905, Brazil
giovanni.amaral@usp.br

Hideyuki Suzuki[3]
Rodolfo T. Gonçalves[3]
[3]Ocean Space Planning Laboratory (OSPL), Department of Systems Innovation, School of Engineering, The University of Tokyo, 7-3-1 Hongo, Bunkyo-ku, Tokyo, 113-8656, Japan
suzukih@sys.t.u-tokyo.ac.jp; goncalves@g.ecc.u-tokyo.ac.jp

Abstract. *A dynamic phenomenon called Vortex-Induced Motion (VIM) is commonly observed in multi-column platforms subject to ocean current, and it can impact the fatigue life of mooring lines and the downtime of Floating Offshore Wind Turbines (FOWT) systems. The present paper deals with a sensitivity analysis of a mathematical Reduced-Order Model (ROM) developed to predict the VIM of FOWTs, comparing the results with reduced-scale experiments carried out in a towing tank facility. The ROM considers the horizontal plane motions (in-line, transverse, and yaw) and nonlinear mooring forces. Current forces are represented using wake oscillator models, represented by forced van der Pol equations, extending previous numerical models constructed initially to assess the VIM of monocolumn platforms. The present ROM is derived by taking 3+2N generalized coordinates, three coordinates for the rigid body motions on the horizontal plane, and two wake variables for each of the N columns. Simulations were conducted for three circular columns FOWT. A parametric variation of hydrodynamic coefficients was performed to investigate the effect of the distance between columns on the VIM response of the FOWT. The highest sensitivity coefficients were identified based on parametric analysis, enabling future calibration of the ROM.*

Keywords: *Vortex-Induced Motions (VIM), Floating Offshore Wind Turbine (FOWT), Reduced-Order Model (ROM), Parametric Analysis, Experimental Comparison*

1. INTRODUCTION

Offshore wind energy, characterized by its high power density, stability, and vast oceanic expanses, has emerged as a promising renewable energy source. In the realm of offshore wind, structures initially designed for oil and gas extraction, such as Tension Leg Platforms (TLP), monocolumn, semi-submersible, and barge-type platforms, are now being repurposed to support wind turbines in mid and deep waters (Díaz *et al*., 2022). These floating platforms face substantial loads from waves, wind, and currents. Dynamics due to the ocean current incidence induce oscillatory motions in the platform and are known as Flow-Induced Motions (FIM), which is crucial to be considered in the early design stages of Floating Offshore Wind Turbines (FOWTs), see (Yin *et al*., 2022; Gonçalves *et al*., 2021). Specific rigid-body motions due to the vortex structures generated surrounding the platform, better known as Vortex-Induced Motions (VIM), is a complex phenomenon falling under the Vortex-Induced Vibration (VIV) category, where vortex-shedding frequencies synchronize with the rigid-body natural frequencies of the floating platform (Fujarra *et al*., 2012).

While Computational Fluid Dynamics (CFD) models, which solve Navier-Stokes and Poisson equations, may be used to predict VIM (Koop *et al*., 2016, 2023; Li *et al*., 2023); however, their extensive computational requirements pose challenges for practical design applications, necessitating thorough verification and validation processes (Wang *et al*. 2021).

An alternative approach involves phenomenological models, like van der Pol equations, suited for modeling vortex wake dynamics. Recent research, in the context of vortex shedding from a circular cylinder, has shown that Ginsburg-Landau equation naturally emerges from the Navier-Stokes equations (Aranha, 2004). In fact, van der Pol Equations are promptly derivable from Landau equation, what gives support to be employed to VIV phenomena and, therefore, to be used to in the coupling of flow and structural dynamics for the VIM phenomenon.

Foundational models from the 1960s and 1970s have been refined over time (Iwan & Blevins, 1974), with recent discussions revisiting concepts such as the added mass effect in VIV (Bernitsas *et al*., 2019; Cunha *et al*., 2006; Facchinetti *et al*., 2004; Fujarra & Pesce, 2002; Skop & Balasubramanian, 1997). Researchers have also developed and enhanced VIV models, expanding from one Degree-of-Freedom (1-DoF) to 2-DoFs models, with modifications based on experimental observations (Franzini & Bunzel, 2018; Postnikov *et al*., 2017; Ogink & Metrikine, 2010).

CFD simulations have been instrumental in calibrating wake oscillator models and exploring factors such as mass ratio's influence on response amplitudes (Postnikov *et al*., 2017). These models have been successfully applied in various floating platforms subjected to VIM, such as Monocolumn Production, Storage, and Offloading (MPSO) platforms (Rosetti *et al*., 2009, 2011), where the platform's low draft and related three-dimensional flow effects significantly affect vortex shedding frequency and the Strouhal number (Gonçalves *et al*., 2009, 2010, 2015).

Advancements in modeling VIM for MPSO platforms include a two-wake oscillators model and a 5-DoFs Reduced Order Model (ROM), which accurately capture platform dynamics and VIM phenomena (Pesce *et al*., 2019). Notably, analytical modeling of mooring line dynamics has revealed yawing motions induced by the mooring lines (Pesce *et al*., 2018). Similarly, the ROM has been developed for multicolumn FOWT, incorporating the rigid body motion of the platform and wake oscillators for each platform column (de Oliveira *et al*., 2021).

To validate the previous ROM models developed by the research group, simulation campaigns have been conducted to replicate experimental studies with reduced-scale platforms (Gonçalves *et al*., 2018, 2021). The ROMs have demonstrated excellent agreement with experimental data, accurately reproducing transverse amplitudes and lock-in regions. Simulations have also unveiled resonant yaw motions at high reduced velocities, confirming experimental observations. A susceptibility model for VIM in FOWTs was also introduced and validated against ROM results (Pesce *et al*., 2021). Furthermore, a comparative analysis between the ROM and a 2D CFD model demonstrated the ROM enhanced predictive capabilities and good computational efficiency (Scopel *et al*., 2023).

The rest of the paper is organized as follows: first, the ROM is briefly summarized, and the selected parameters for the sensitivity study are presented. Next, case studies are outlined, and results are discussed. Finally, conclusions and devised further work are drawn.

2. REDUCED ORDER MODEL

The detailed deduction of the ROM may be seen in de Oliveira *et al*. (2021). The ROM was developed considering the motion of the platform restricted to the horizontal plane. The platform is taken as a rigid body. The ROM is derived from Lagrange's equations with 3-DoFs. The hydrodynamic interaction is emulated through a phenomenological model based on wake oscillators (Franzini & Bunzel, 2018), based on (Ogink & Metrikine, 2010). A pair of oscillators are applied to each column, so the generalized coordinate vector is expanded to 3+2*N* degrees of freedom, being *N* the number of columns.

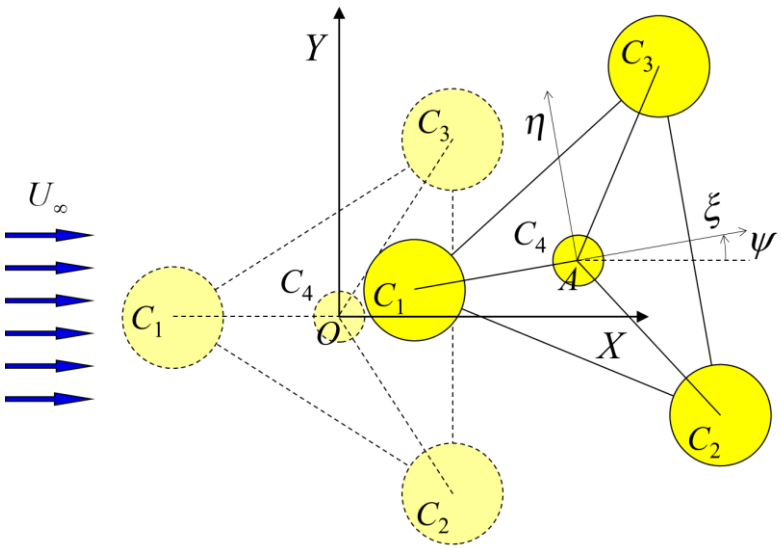

Figure 1. Coordinates and general definitions. At the origin, the platform is shown at 0 degrees current heading.

Therefore, the resulting 3+2*N*-DoFs ROM may be written in the following form:

$$\tilde{\mathbf{M}}\ddot{\tilde{\mathbf{q}}} + \mathbf{Q}^I = \tilde{\mathbf{Q}}_c + \tilde{\mathbf{Q}}_{nc}, \tag{1}$$

where $\tilde{\mathbf{M}}$ and $\tilde{\mathbf{q}}$ are, respectively, the augmented inertia matrix and generalized coordinate vector, $\mathbf{Q}^I$ are inertial non-linear terms, and, on the r.h.s., $\tilde{\mathbf{Q}}_c$ and $\tilde{\mathbf{Q}}_{nc}$ are, respectively, extended generalized force vectors, the first one dependent on the generalized configuration of the system and the second one on non-conservative terms. Their explicit forms are:

$$\tilde{\mathbf{q}} = \begin{bmatrix} \mathbf{q} \\ \mathbf{w} \end{bmatrix}; \quad \tilde{\mathbf{M}} = \begin{bmatrix} \mathbf{M} & \mathbf{0} \\ \mathbf{A}_w & \mathbf{1} \end{bmatrix}; \quad \tilde{\mathbf{Q}}_c = \begin{bmatrix} \mathbf{Q}^m \\ \mathbf{Q}^r_w \end{bmatrix}; \quad \tilde{\mathbf{Q}}_{nc} = \begin{bmatrix} \mathbf{Q}^v \\ \mathbf{Q}^v_w \end{bmatrix}, \tag{2}$$

where, $\mathbf{q}$ is the (3×1) vector of generalized coordinates of the platform, (X, Y, ψ); $\mathbf{w}$ is the $(2N\times1)$ wake oscillators variables vector; $\mathbf{M}$ is the (3×3) inertia matrix of the platform, including rigid body and added mass parcels[1]; $\mathbf{A}_w$ is the $(2N\times2N)$ matrix of inertial terms coupling the oscillators variables with the columns centers kinematics; $\mathbf{Q}^m$ and $\mathbf{Q}^v$ are, respectively, the (3×1) vectors associated to the generalized mooring forces and vortical viscous forces; $\mathbf{Q}^r_w$ and $\mathbf{Q}^v_w$ are the corresponding $(2N\times1)$ vectors of restoring and damping effects related to the wake oscillators dynamics.

The wake oscillator models for each column *k*, $k = 1,\ldots,N$, are written in the respective local in-line and transverse directions, (ξ,η), as presented below:

$$\begin{aligned} &\ddot{w}_{\xi,k} + \varepsilon_\xi \omega_{s,k}(w^2_{\xi,k} - 1)\dot{w}_{\xi,k} + 4\omega^2_{s,k} w_{\xi,k} = \frac{A_\xi}{D_k} a_{\xi,k}, \\ &\ddot{w}_{\eta,k} + \varepsilon_\eta \omega_{s,k}(w^2_{\eta,k} - 1)\dot{w}_{\eta,k} + \omega^2_{s,k} w_{\eta,k} = \frac{A_\eta}{D_k} a_{\eta,k}, \end{aligned} \tag{3}$$

where $w_{\xi,k}$ and $w_{\eta,k}$ ($k = 1,\ldots,N$) are the hidden generalized coordinates that phenomenologically emulate the wake dynamics and its interaction with the structure; ε_ξ and ε_η are damping parameters; A_ξ and A_η are the inertial coupling parameters, as per (Franzini & Bunzel, 2018), according to (Ogink & Metrikine, 2010), after (Facchinetti *et al*., 2004); D_k is the column diameter; $a_{\xi,k}$ and $a_{\eta,k}$ are the body-fixed components of the columns accelerations and $\omega_{s,k} = 2\pi S_{t,k}\left(U_k / D_k\right)$ is the shedding frequency, with $S_{t,k}$ as the characteristic value of the Strouhal number for the case of low aspect ratio cylinders, and U_k is the relative velocity of the column centroid with respect to the flow. Notice that the in-line wake oscillator is assumed to vibrate with twice the frequency of the transverse one. This is a common *ad-hoc* assumption from experimental VIV observations, according to which the fundamental harmonic of hydrodynamic drag forces pulsates twice as fast as that of the lift forces. The coefficients $(\varepsilon_\xi, \varepsilon_\eta)$ and (A_ξ, A_η) have been calibrated from experiments (Rosetti *et al*., 2009, 2011) and from CFD simulations (Postnikov *et al*., 2017). Tables 1 to 5 show the ROM parameters.

Recall that in the VIV technical literature, involving wake-oscillators, some possibilities of coupling have been tested. Some involve velocities, some involve inertial terms (acceleration), some involve both. Within the Franzini & Bunzel, 2018) approach, which is based on the (Ogink & Metrikine, 2010) model, inertial coupling is considered the best approach, after the investigation by (Facchinetti et al., 2004). In fact, this approach is consistent with the concept of variable added mass with reduced velocity thoroughly discussed in the VIV literature.

The generalized vortical viscous forces are computed with lift and drag coefficients for each column *k*, $k = 1,\ldots,N$, written as functions of the wake variables (Postnikov *et al*., 2017; Rosetti *et al*., 2009), as follows:

$$\begin{aligned} &C_{L,k} = \frac{C_{L0}}{2} w_{\eta,k}, \\ &C_{D,k} = C_{D0}\left(1 + K_f w^2_{\eta,k}\right) + \frac{C_{f,D0}}{2} w_{\xi,k}, \end{aligned} \tag{4}$$

where C_{L0} and C_{D0} are, respectively, the lift and drag coefficients for a fixed cylinder; C^f_{D0} is a weighting coefficient for the oscillation amplitude of the drag; and K_f is a constant, experimentally determined (Rosetti *et al*., 2009). The influence of these parameters on the motion amplitudes and dominant oscillation frequencies will be assessed next.

[1] The added mass matrix is determined from the potential flow theory, taking the zero-frequency asymptotic limit, where free surface effects are negligible. Both matrices, the body's and the added mass', are calculated in the body reference frame (ξ,η) and rotated to the inertial frame at each instant of time.

3. RESULTS

To perform the parametric analysis, a case study was carried out considering the reduced scale model of three-column platforms (see Figure 2) with a simplified mooring system composed of 4 spring lines connected to the towing carriage, shown in Figure 3 (a) and presented by Gonçalves *et al*. (2020). The results presented herein try to replicate the experiments on a reduced scale, where three different column distances were considered (S/L = 2, 3, 4), as illustrated in Figure 3 (b)-(d). Geometrically nonlinear effects of the mooring system were duly considered. Simulations were carried out at least for 60 reduced velocities, spanning the range $0 < V_R < 30$, corresponding to the Reynolds number interval 10,000 < Re < 110,000, for each column distance. The simulations were conducted in a MATLAB® environment, numerically integrating the coupled equations in the state space form. A fixed time step of 0.1 seconds was used, applying the 4th-order Runge-Kutta algorithm. The parameters selected for the sensitivity study refer to the base hydrodynamic coefficients of Eq. (4) as commented before, i.e., C_{D0}^{f}, C_{L0}, C_{D0} and K_f.

The platform's main characteristics are shown in Table 2, while the mooring system parameters and those corresponding to the wake oscillators are given in Tables 2 and 3, respectively. Table 4 shows the inertia and stiffness matrices calculated at the trivial equilibrium position for the column distances considered in the reduced-scale experiment. In contrast, Table 5 shows the three natural periods evaluated at the same trivial equilibrium condition, comparing the experimentally measured with those calculated with the ROM. Notice that the oscillation modes are pure at the trivial equilibrium, uncoupling the (X, Y, ψ) degrees of freedom. As the platform model drifts off from that trivial equilibrium position, mooring forces change nonlinearly, and motions couple to each other, producing yaw, even if the current is aligned initially with an axis of symmetry.

Table 1. Three columns platform scaled model parameters (Gonçalves *et al*., 2020).

Parameters	Values
Draught, H [m]	0.38
Arc radius, R [m]	0.66
Columns centers' radius, r [m]	0.29
Diameters, $\{D_1, D_2, D_3\}$ [m]	{0.25, 0.25, 0.25}
Platform's mass, m_p [kg]	55.20
Platform's inertia (S / L = 2, 3, 4), I_p [kgm²]	10.30, 16.12, 24.32
Platform's mass matrix, $\mathbf{M}_p$ [kg, kg, kgm²]	diag{m_p, m_p, I_p}
Platform's added mass, m_a [kg]	36.34
Platform's added inertia (S / L = 2, 3, 4), I_a [kgm²]	3.03, 6.81, 12.11
Added mass tensor in the moving frame, $\hat{\mathbf{M}}_a$ [kg, kg, kgm²]	diag{m_a, m_a, I_a}
Density of water, ρ [kg/m³]	997

Table 2. Mooring system parameters (Gonçalves *et al*., 2020).

Parameters	Values
Towing car dimensions, $\{W_m, L_m, \Phi_m\}$ [m]	{1.43, 2.35, 1.32}
Natural lengths, $\{l_{n_1}, l_{n_2}, l_{n_3}, l_{n_4}\}$ [m]	{0.84, 0.35, 0.84, 0.35}
Spring constants, $\{k_1, k_2, k_3, k_4\}$ [N/m]	{7.85, 9.51, 7.85, 9.51}

Table 3. Wake-oscillators parameters (Gonçalves *et al*., 2015; Rosetti *et al*., 2009)

Parameters	Values
Inertial coupling parameters, $\{A_\xi, A_\eta\}$	{12, 6}
Damping parameters, $\{\varepsilon_\xi, \varepsilon_\eta\}$	{0.30, 0.15}
Hydrodynamic coefficients (reference values), $\{C_{D0}, C_{L0}, C_{f,D0}, K_f\}$	{0.70, 0.30, 0.10, 0.05}
Strouhal numbers for each column, $\{S_{t_1}, S_{t_2}, S_{t_3}\}$	{0.14, 0.14, 0.14}

Table 4. Mass and stiffness matrices at the trivial equilibrium position (Gonçalves *et al*., 2020).

Parameters	Values
Mass matrix (S / L = 2, 3, 4), **M** [kg, kg, kgm²]	diag{91.54, 91.54, 13.33} diag{91.54, 91.54, 22.93} diag{91.54, 91.54, 36.43}
Mooring stiffness matrix, **K** [N/m, N/m, Nm]	diag{25.86, 26.98, 22.23}

Table 5. Natural periods at the trivial equilibrium position (Gonçalves *et al*., 2020).

DOF	Experiment, T_n [s]			ROM, T_n [s]		
	S / L = 2	S / L = 3	S / L = 4	S / L = 2	S / L = 3	S / L = 4
X	13.5	13.2	12.9	11.83	11.83	11.83
Y	13.6	13.3	12.8	11.57	11.57	11.57
ψ	3.7	5.6	5.6	4.86	6.37	8.03

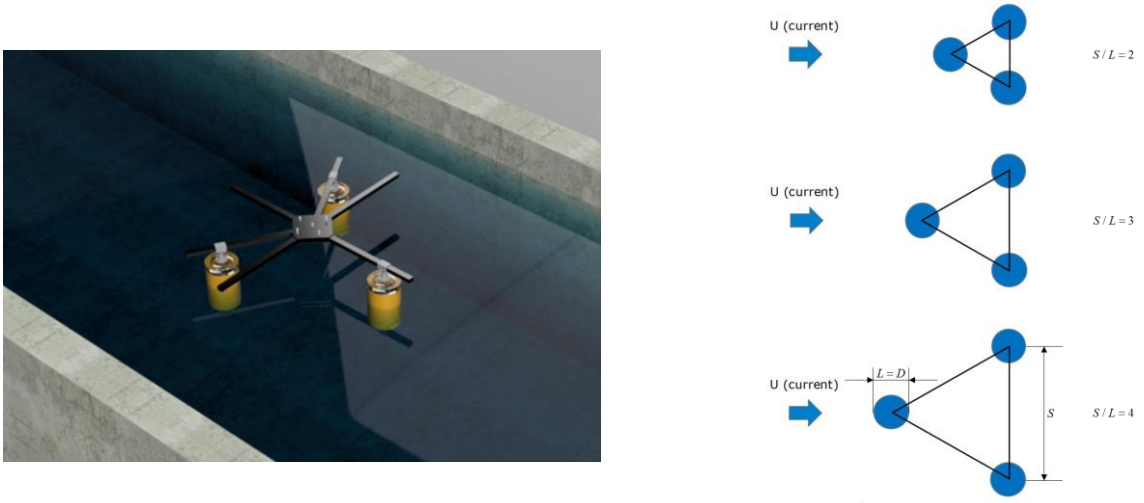

(a) (b)

Figure 2. Schematic diagram of the 3-column platform. (a): Scale model; (b): Configurations for different column distances (S/L = 2, 3, 4). Adapted from Gonçalves *et al*. (2020).

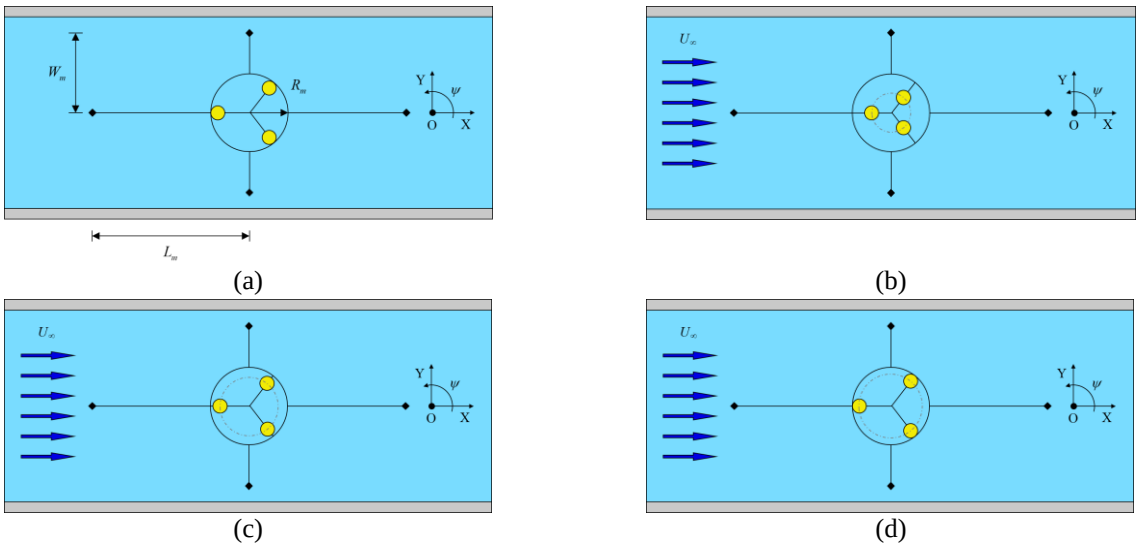

(a) (b)

(c) (d)

Figure 3. Experiment sketch with the simplified mooring system. (a): tank sketch and mooring system geometry. (b): Incoming flow incidence at 0 degrees and for S/L = 2. (c): Incoming flow incidence at 0 degrees and for S/L = 3. (d): Incoming flow incidence at 0 degrees and for S/L = 4. Adapted from de Oliveira *et al*. (2021).

Figures 4 to 7 compare the nondimensional amplitudes obtained with the ROM and the experimental results presented in Gonçalves *et al*. (2020). Nondimensional amplitude responses and dominant oscillating frequencies are shown as a function of the reduced velocity, $V_R = U/f_n D$, where $D = L$ is the diameter of the columns, and $f_n = f_Y$ is the natural frequency related to the transverse motion at the trivial equilibrium. High reduced velocities could not be achieved during the experiments due to the drag forces, which produced excessive platform drift; therefore, the experimental data are available only for lower reduced velocities varying from $5 < V_R < 13$, $5 < V_R < 10$ and $4 < V_R < 7$ for S/L = 2, 3, 4, respectively.

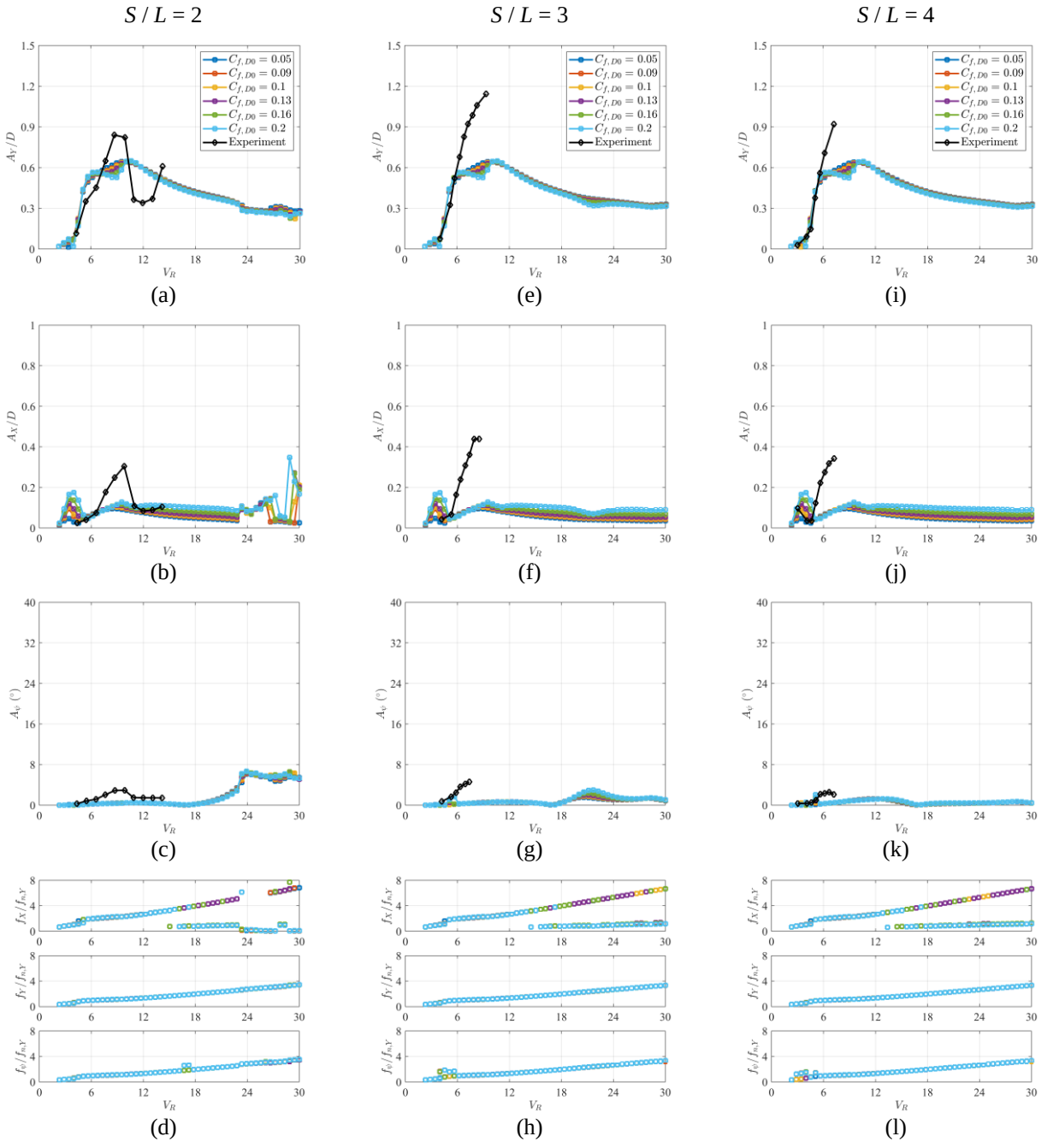

Figure 4. Parametric analysis for $C_{f,D0}$ and comparison with experimental results (Gonçalves *et al*., 2020). Flow at 0 degrees incidence. (a)-(d): S/L = 2, (e)-(h): S/L = 3, (i)-(l): S/L = 4. (a), (e), (i): Transverse amplitude; (b), (f), (j): In-line amplitude; (c), (g), (k): Yaw amplitude; (d), (h), (l): Dominant nondimensional frequencies.

Concerning the sensitivity study regarding the hydrodynamic coefficients, C_{D0}^f, it was revealed to be the least essential coefficient, producing minimal variation of the amplitudes, as seen in Figure 4. On the other hand, C_{L0} and C_{D0} had a high influence on the nondimensional amplitudes, producing high variation in the transverse directions but also affecting

in-line and yaw motions, as seen in Figures 5 and 6. Therefore, its calibration could be complex once a minor change can result in undesirable variations in motion directions other than the desired one.

The coefficient K_f also influenced the amplitudes, especially in the transverse direction, as seen in Figure 7. Thus, it can be an option to calibrate the transverse amplitudes directly. As expected, the dominant nondimensional frequencies in Figures 4, 5, 6, and 7 (d), (h), and (l) did not change significantly with the variation of the hydrodynamic coefficients. The slight variation was due to the platform drifting, changing the equilibrium position, which increased with the reduced velocity and affected the mooring stiffness matrix.

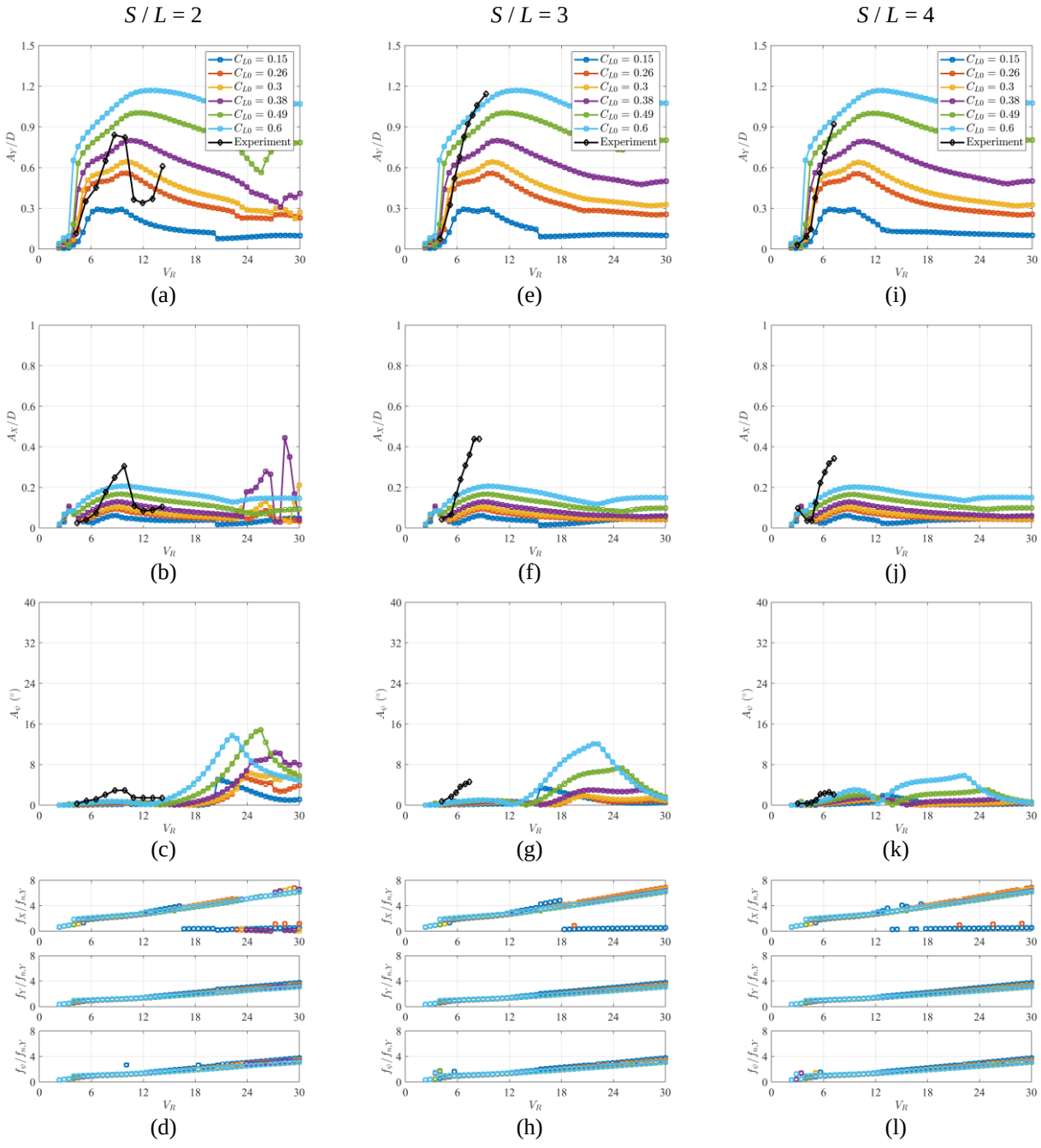

Figure 5. Parametric analysis for C_{L0} and comparison with experimental results (Gonçalves *et al*., 2020). Flow at 0 degrees incidence. (a)-(d): S/L = 2, (e)-(h): S/L = 3, (i)-(l): S/L = 4. (a), (e), (i): Transverse amplitude; (b), (f), (j): In-line amplitude; (c), (g), (k): Yaw amplitude; (d), (h), (l): Dominant nondimensional frequencies.

Comparing the sensitivity study of C_{L0} and C_{D0} in Figures 5 and 6 (a), (e) and (i), we can see an almost uniform variation for the transverse amplitudes. However, in Figure 6 (a), (b), and (c) for S/L = 2, there is a peak in the amplitudes associated with a very low C_{D0} value. The same behavior is seen in Figure 6 (a), (b), and (c) for S/L = 3, but now reduced,

indicating that such an effect was associated with the inertia moment of the platform. Similar behavior was observed for the other coefficients but with lower intensity. Also, the model reproduced the transverse amplitudes of the experiments very well for reduced velocities ranging from $5 < V_R < 13$, $5 < V_R < 10$ and $4 < V_R < 7$ for S/L = 2, 3, 4, respectively. However, conclusive observations cannot be made due to incomplete experimental data for high reduced velocities.

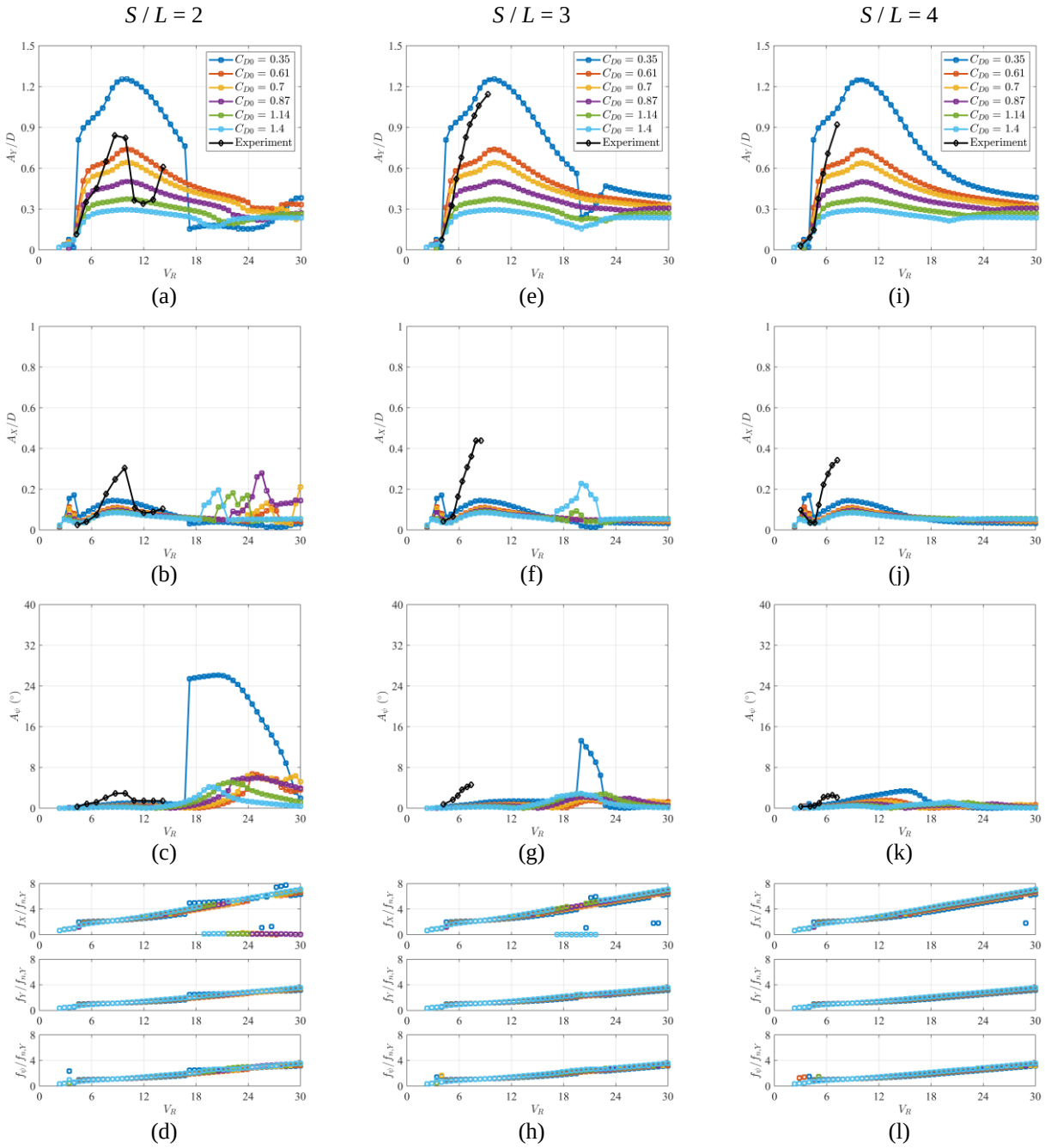

Figure 6. Parametric analysis for C_{D0} and comparison with experimental results (Gonçalves *et al.*, 2020). Flow at 0 degrees incidence. (a)-(d): S/L = 2, (e)-(h): S/L = 3, (i)-(l): S/L = 4. (a), (e), (i): Cross flow amplitude; (b), (f), (j): In-line amplitude; (c), (g), (k): Yaw amplitude; (d), (h), (l): Dominant nondimensional frequencies.

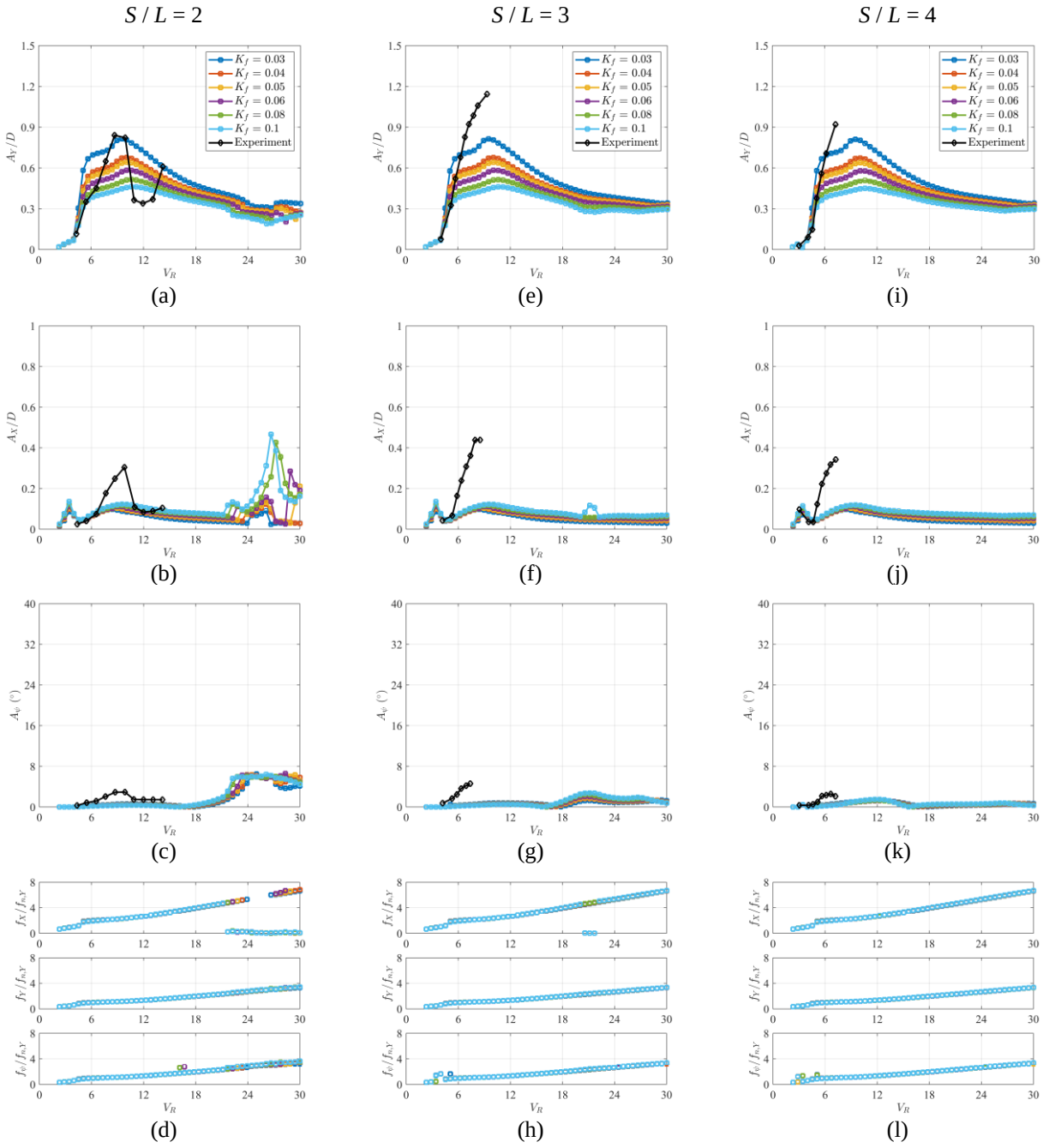

Figure 7. Parametric analysis for K_f and comparison with experimental results (Gonçalves *et al.*, 2020). Flow at 0 degrees incidence. (a)-(d): S/L = 2, (e)-(h): S/L = 3, (i)-(l): S/L = 4. (a), (e), (i): Cross flow amplitude; (b), (f), (j): In-line amplitude; (c), (g), (k): Yaw amplitude; (d), (h), (l): Dominant nondimensional frequencies.

4. CONCLUSIONS

A reduced order model (ROM) to predict the VIM of FOWTs, previously derived in (de Oliveira *et al.*, 2021), was discussed. The ROM focuses on obtaining the oscillatory motions in the horizontal plane at low frequencies. The ROM considers a pair of van der Pol-type wake oscillators for each FOWT column to capture the effects of viscous fluid forces induced by vortex shedding. These oscillators represent the dynamics of the vortex wake shed from each cylindrical column and respond to the local relative velocity of the incoming flow with respect to the column centroid. Presently, the model simplifies the analysis by neglecting wake interferences among columns. Base parameters for the wake oscillators were taken from the technical literature, while Strouhal numbers were obtained from experimental results involving low-aspect-ratio cylinders. The choice of the Strouhal number as a function of the aspect ratio of the cylinders is a crucial and subtle aspect, since, in a sense, it incorporates three-dimensional effects of the flow.

The sensitivity study revealed that the most important hydrodynamic coefficients for the ROM calibration are C_{L0}, C_{D0} and K_f. Furthermore, C_{L0} and C_{D0} influence all motions while K_f has a dominant effect on the transverse amplitude, which can simplify further calibration. Future work should involve Physics-Based Machine Learning techniques, in search of a more general application model for a family of floating platforms with multiple circular columns, with and without pontoons.

ACKNOWLEDGMENTS

The Petrobras Deep Water Floating Offshore Wind Turbine project is acknowledged for partially supporting the present work. The second author acknowledges a research grant from CNPq, process 307995/2022-4. The São Paulo State Research Foundation (FAPESP) is also acknowledged for supporting the Thematic Project "Nonlinear Dynamics applied to Engineering Systems", process 2022/00770-0.

REFERENCES

Aranha, J. A. P. (2004). Weak three dimensionality of a flow around a slender cylinder: The ginzburg-landau equation. *Journal of the Brazilian Society of Mechanical Sciences and Engineering*, *26*(4), 355–367. https://doi.org/10.1590/S1678-58782004000400002

Bernitsas, M. M., Ofuegbe, J., Chen, J.-U., & Sun, H. (2019). Eigen-Solution for Flow Induced Oscillations (VIV and Galloping) Revealed at the Fluid-Structure Interface. *38th International Conference on Ocean, Offshore and Arctic Engineering; Volume 2: CFD and FSI*, 21. https://doi.org/10.1115/OMAE2019-96823

Cunha, L. D., Pesce, C. P., Wanderley, J., & Fujarra, A. L. C. (2006). The Robustness of the Added Mass in VIV Models. *Volume 4: Terry Jones Pipeline Technology; Ocean Space Utilization; CFD and VIV Symposium*, 731–738. https://doi.org/10.1115/OMAE2006-92323

de Oliveira, É. L., Pesce, C. P., Mendes, B., Orsino, R. M. M., & Franzini, G. R. (2021). A Reduced-Order Mathematical Model for the Current-Induced Motion of a Floating Offshore Wind Turbine. *ASME 2021 3rd International Offshore Wind Technical Conference*, 1–11. https://doi.org/10.1115/IOWTC2021-3503

Díaz, H., Serna, J., Nieto, J., & Soares, C. G. (2022) "Market Needs, Opportunities and Barriers for Floating Wind Industry," *Journal of Marine Science and Engineering*, 10, 934. https://doi:10.3390/jmse10070934

Facchinetti, M. L., de Langre, E., & Biolley, F. (2004). Coupling of structure and wake oscillators in vortex-induced vibrations. *Journal of Fluids and Structures*, *19*(2), 123–140. https://doi.org/10.1016/j.jfluidstructs.2003.12.004

Franzini, G. R., & Bunzel, L. O. (2018). A numerical investigation on piezoelectric energy harvesting from Vortex-Induced Vibrations with one and two degrees of freedom. *Journal of Fluids and Structures*, *77*, 196–212. https://doi.org/10.1016/j.jfluidstructs.2017.12.007

Fujarra, A. L. C., & Pesce, C. P. (2002). Added Mass Variation and Van der Pol Models Applied to Vortex-Induced Vibrations. *5th International Symposium on Fluid Structure Interaction, Aeroelasticity, and Flow Induced Vibration and Noise*, 207–211. https://doi.org/10.1115/IMECE2002-32162

Fujarra, A. L. C., Rosetti, G. F., de Wilde, J., & Gonçalves, R. T. (2012). State-of-Art on Vortex-Induced Motion: A Comprehensive Survey After More Than One Decade of Experimental Investigation. *Volume 4: Offshore Geotechnics; Ronald W. Yeung Honoring Symposium on Offshore and Ship Hydrodynamics*, 561–582. https://doi.org/10.1115/OMAE2012-83561

Gonçalves, R. T., Matsumoto, F. T., Malta, E. B., Rosetti, G. F., Fujarra, A. L. C., & Nishimoto, K. (2009). Evolution of the MPSO (monocolumn production, storage and offloading system). *Marine Systems & Ocean Technology*, *5*(1), 45–53. https://doi.org/10.1007/BF03449242

Gonçalves, R. T., Fujarra, A. L. C., Rosetti, G. F., & Nishimoto, K. (2010) "Mitigation of Vortex-Induced Motion (VIM) on a Monocolumn Platform: Forces and Movements," *Journal of Offshore Mechanics and Arctic Engineering*, 132, 041102. https://doi.org/10.1115/1.4001440

Gonçalves, R. T., Franzini, G. R., Rosetti, G. F., Meneghini, J. R., & Fujarra, A. L. C. (2015). Flow around circular cylinders with very low aspect ratio. *Journal of Fluids and Structures*, *54*, 122–141. https://doi.org/10.1016/j.jfluidstructs.2014.11.003

Gonçalves, R. T., Fujarra, A. L. C., Rosetti, G. F., Kogishi, A. M., & Koop, A. (2018). Experimental study of the column shape and the roughness effects on the vortex-induced motions of deep-draft semi-submersible platforms. *Ocean Engineering*, *149*, 127–141. https://doi.org/10.1016/j.oceaneng.2017.12.013

Gonçalves, R. T., Chame, M. E. F., Hannes, N. H., Lopes, P. P. S. de P., Hirabayashi, S., & Suzuki, H. (2020). FIM – Flow-Induced Motion of Three-Column Platforms. *International Journal of Offshore and Polar Engineering*, *30*(2), 177–185. https://doi.org/10.17736/ijope.2020.mt25

Gonçalves, R. T., Chame, M. E. F., Silva, L. S. P., Koop, A., Hirabayashi, S., and Suzuki, H. (2021) "Experimental flow-induced motions (FIM) of a FOWT semi-submersible type (OC4 phase II floater)," *Journal of Offshore Mechanics and Arctic Engineering*, 143, 012004. https://doi.org/10.1115/1.4048149

Koop, A., Vaz, G., Maximiano, A., & Rosetti, G. F. (2016) "CFD investigation on scale and damping effects for vortex induced motions of a semi-submersible floater," In *Proceedings of the Offshore Technology Conference*, OTC-26977-MS, Houston, TX, USA. https://doi.org/10.4043/26977-MS

Koop, A., Leverette, S., Bangs, A., Withall, T., Valverde, F. C., der Zanden, J. V., Heerink, R, & de Wilde, J. (2023) "Investigating the effect of damping originating from mooring and risers on the VIM response of a semi-submersible floater using coupled CFD-time-domain simulations," In *Proceedings of the Offshore Technology Conference*, OTC-32285-MS, Houston, TX, USA. https://doi.org/10.4043/32285-MS

Iwan, W. D., & Blevins, R. D. (1974). A Model for Vortex Induced Oscillation of Structures. *Journal of Applied Mechanics*, *41*(3), 581–586. https://doi.org/10.1115/1.3423352

Li, X., Xiao, Q., Wang, E., Peyrard, C., & Gonçalves, R. T. "The Dynamic response of Floating Offshore Wind Turbine Platform in Wave-Current Condition," *Physics of Fluids*, 35, 087113. https://doi.org/10.1063/5.0158917

Ogink, R. H. M., & Metrikine, A. V. (2010). A wake oscillator with frequency dependent coupling for the modeling of vortex-induced vibration. *Journal of Sound and Vibration*, *329*(26), 5452–5473. https://doi.org/10.1016/j.jsv.2010.07.008

Pesce, B., de Oliveira, É. L., & Pesce, C. P. (2019). Vortex Induced Motions of a Moored Monocolumn Platform. *DINAME2019*. https://doi.org/10.26678/ABCM.DINAME2019.DIN2019-0213

Pesce, C. P., Amaral, G. A., & Franzini, G. R. (2018). Mooring system stiffness: A general analytical formulation with an application to floating offshore wind turbines. *ASME 2018 1st International Offshore Wind Technical Conference, IOWTC 2018*, 1–12. https://doi.org/10.1115/IOWTC2018-1040

Pesce, C. P., Amaral, G. A., Mendes, B., Oliveira, E. L., & Franzini, G. R. (2021). A Model to Assess the Susceptibility of a Multicolumn FOWT Platform to Vortex-Induced Motions in Early Design Stages. *Volume 9: Ocean Renewable Energy*, 1–10. https://doi.org/10.1115/OMAE2021-65761

Postnikov, A., Pavlovskaia, E., & Wiercigroch, M. (2017). 2DOF CFD calibrated wake oscillator model to investigate vortex-induced vibrations. *International Journal of Mechanical Sciences*, *127*, 176–190. https://doi.org/10.1016/j.ijmecsci.2016.05.019

Rosetti, G. F., Gonçalves, R. T., Fujarra, A. L. C., Nishimoto, K., & Ferreira, M. D. (2009). A Phenomenological Model for Vortex-Induced Motions of the Monocolumn Platform and Comparison With Experiments. *Volume 1: Offshore Technology*, 437–444. https://doi.org/10.1115/OMAE2009-79431

Rosetti, G. F., Gonçalves, R. T., Fujarra, A. L. C., & Nishimoto, K. (2011). Parametric analysis of a phenomenological model for vortex-induced motions of monocolumn platforms. *Journal of the Brazilian Society of Mechanical Sciences and Engineering*, *33*(2), 139–146. https://doi.org/10.1590/S1678-58782011000200004

Scopel, A. X., de Oliveira, É. L., Carmo, B. S., & Pesce, C. P. (2023). Vortex-Induced Motion of a Multicolumn Floating Offshore Wind Turbine Platform: A Study Comparing Two Modelling Approaches – CFD and a Reduced Order Model. *Proceedings of 27th ABCM International Congress of Mechanical Engineering*, 11. https://doi.org/10.26678/ABCM.COBEM2023.COB2023-1968

Skop, R. A., & Balasubramanian, S. (1997). A New Twist on an Old Model for Vortex-Excited Vibrations. *Journal of Fluids and Structures*, *11*(4), 395–412. https://doi.org/10.1006/jfls.1997.0085

Wang, Y., Chen, H-C., Koop, A., & Vaz, G. (2021) "Verification and validation of CFD simulations for semi-submersible floating offshore wind turbine under pitch free-decay motion," *Ocean Engineering*, 242, 109993. https://doi.org/10.1016/j.oceaneng.2021.109993

Yin, D., Passano, E., Jiang, F., Lie, H., Wu, J., Ye, N., Saevik, S., & Leira, B. J. (2022) "State-of-the-art review of vortex-induced motions of floating offshore wind turbine structures," *Journal of Marine Science and Engineering*, 10, 1021. https://doi.org/10.3390/jmse10081021